Appl. Phys. A (2016) 122:1027
DOI 10.1007/s00339-016-0569-7

Applied Physics A
Materials Science & Processing

Structural, electrical, band alignment and charge trapping analysis of nitrogen-annealed Pt/HfO_2/p-Si (100) MIS devices

Arvind Kumar[1] · Sandip Mondal[1] · K. S. R. Koteswara Rao[1]

Received: 23 June 2016 / Accepted: 11 November 2016 / Published online: 17 November 2016

Abstract Low leakage current density and high relative permittivity (dielectric constant) are the key factor in order to replace the SiO_2 from Si-based technology toward its further downscaling. HfO_2 thin films received significant attention due to its excellent optoelectronic properties. In this work, ultra-thin (17 nm) HfO_2 films on Si substrate are fabricated by RF sputtering. As deposited films are amorphous in nature and in order to get the reasonable high dielectric constant, the films are annealed (700 °C, 30 min) in nitrogen environment. A high refractive index (2.08) and small grain size ($\sim$10) nm were extracted from ellipsometry and XRD, respectively. The AFM study revealed a small RMS surface roughness 9 Å. For electrical characterization, films are integrated in metal–insulator–semiconductor capacitors structure. The oxide capacitance (C_{ox}), flat band capacitance (C_{FB}), flat band voltage (V_{FB}), and oxide-trapped charges (Q_{ot}) calculated from high-frequency (1 MHz) C–V curve are 490, 241 pF, 1.21 V and 1.8×10^{12} cm^{-2}, respectively. The dielectric constant calculated from accumulation capacitance is 17. The films show a low leakage current density 6.8×10^{-9} A/cm^2 at +1 V, and this is due to the reduction in oxygen vacancies concentration as we performed annealing in N_2 environment. The band gap of the films is estimated from O 1s loss spectra and found 5.7 eV. The electron affinity (χ) and HfO_2/Si barrier height (conduction band offset) extracted from UPS spectra are 1.88 and 2.17 eV, respectively. A trap state with 0.99 eV activation energy below the conduction band edge is found and assigned to the fourfold coordinated oxygen vacancy in m-HfO_2.

✉ Arvind Kumar
arvind@physics.iisc.ernet.in

[1] Department of Physics, Indian Institute of Science, Bangalore 560012, India

1 Introduction

The downscaling of electronic devices has headed the SiO_2 layer used as a gate dielectric becoming so thin that the gate leakage current becomes too large [1]. This led to the replacement of SiO_2 by a physically thicker layer of a higher dielectric constant or 'high-κ' oxide such as TiO_2, ZrO_2 and HfO_2 or may be their combinations [2, 3]. Among all these high-k, HfO_2 is a promising functional material and has received significant attention due to its fascinating physicochemical-optoelectronic properties. HfO_2 has high dielectric constant ($\sim$30), large band gap (5–6 eV) and excellent thermodynamic stability [4]. In addition to that, it has a large conduction and valence band offset to silicon, which is essential to maintain the requirement of low leakage current density. There are an increasing interest of using HfO_2 as the gate dielectric in thin-film transistors (TFTs) with metal oxides such as zinc oxide (ZnO) and indium gallium zinc oxide (IGZO), channel layers [5, 6]. The fabrication of HfO_2 films by electron beam evaporation, ion-assisted electron beam evaporation, sputtering, chemical vapor deposition and atomic layer epitaxy is broadly explored [7–10]. Recently HfO_2 dielectric layer also shows the potential of its use in TFT and sensor application with higher mobility channel layer using two-dimensional materials (graphene and MoS_2) [8, 11–14]. Organic semiconductor (P3HT, pentacene)-based TFT with HfO_2 dielectrics layer has been reported previously [15–17]. Zhang et al. [18]

reported the ALD HfO_2 deposition process on the Ge substrate. Insulating films fabricated at room temperature exhibit inferior properties and higher leakage current because of the several traps existent of within the film and interface of Si/HfO_2. Hence, high-temperature annealing (600–800 °C, 1 h) is traditionally required to improve the electrical properties of such thin films [19]. Higher-temperature annealing for sufficiently long time may grow the thicker interfacial layer. This will lower the effective dielectric constant of gate stack. On the other hand, annealing in nitrogen atmosphere may reduce the density of traps present in MIS stack and help to reduce the interlayer thickness. The effect of nitrogen (N_2) ambient annealing on structural characteristic of HfO_2 film has been investigated previously [20]. The results of these studies show that the crystallization temperature of HfO_2 gate dielectric is improved by the nitrogen ambient during post-deposition annealing (PDA) process.

In the present work, we investigate the 30-min N_2 annealed ultra-thin (17 nm) films deposited by RF sputtering technique. The structural, electrical and dielectric properties of thus prepared HfO_2 thin films have been investigated on the MIS device structure.

2 Experimental

2.1 Fabrication of MIS devices

Nano-crystalline HfO_2 thin films were fabricated on the *p*-type Si (100) substrates held at room temperature by sputtering of HfO_2 target (99.99 % pure) in an optimized oxygen partial pressure of 0.03 Pa and sputtering power of 60 W. The target to substrate distance was fixed at 7.5 cm. The sputtering chamber was evacuated to an ultimate vacuum of 5×10^{-6} Torr before admitting the reactive gas into the system. Prior to the deposition, the target was sputter cleaned in pure argon atmosphere to remove contaminations from the target surface. Thickness of the films are monitored by quartz crystal oscillator and later verified with ellipsometry technique. Prior to the deposition, Si wafer was cleaned with piranha solution (H_2SO_4:H_2O_2 3:1) followed by dipping with 1 % HF for 10 s to remove any native oxide layer present and then dried using N_2 gas. The films were annealed in a pre-heated furnace in N_2 atmosphere (700 °C, 30 min). The electrical measurements were carried out using 150-nm-thick Pt top electrodes obtained by sputtering. A metal mask was used to pattern the gate area. We have fabricated a lot (70–80 devices) of MIS devices to check the quality and reproducibility.

2.2 Characterizations

The X-ray diffraction (XRD) patterns have been recorded with Rigaku X-ray diffractometer over a 2θ range of 20°–70° in grazing incidence X-ray diffraction (GIXRD) mode. The operating voltage and current was 40 kV and 30 mA, respectively. Ellipsometry data were measured with variable angle spectrometer (M-2000, J.A. Woollam Co., Inc., USA). Atomic force microscopy (AFM) was used for roughness analysis. X-ray photoelectron spectroscopy measurements were recorded with an AXIS ULTRA from AXIS 165 using monochromatized Al Kα as the excitation source. The binding energies are calibrated to surface adventitious carbon (284.4 eV). The band gap of HfO_2 is estimated from the O 1*s* energy loss spectrum. The ultraviolet photoemission spectroscopy (UPS) was used for the determination of electron affinity of HfO_2. Agilent 4294A Precision Impedance Analyzer unit was used to record capacitance–voltage (*C*–*V*) and current–voltage (*J*–*V*) characteristics. The electrical measurements were repeated after few months to check the reproducibility of the MIS devices.

3 Results and discussion

Figure 1 depicts the grazing incidence X-ray diffraction (GIXRD) pattern of 700 °C-annealed HfO_2 films. GIXRD mode is preferred due to small thickness of the films. An intense peak at $2\theta = 28.47$ is observed, which revealed the crystallized monoclinic phase of HfO_2. The average grain size calculated using dominating (−111) plane and Debye–

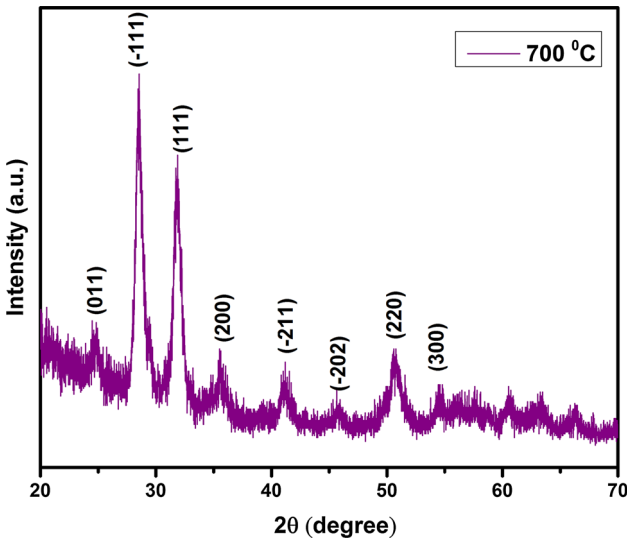

Fig. 1 GIXRD patterns of 700 °C-nitrogen-environment-annealed HfO_2 films. The film shows a monocline phase of HfO_2

Scherrer formula was found to be 10 nm. The other peaks are marked in the plot according to JCPDS card [21].

Surface roughness is an important factor towards the use of thin films in electronics device. A rough surface can trap the carrier and degrades the device performance. Hence, a fairly small surface roughness is desirable for device application. The AFM image of HfO_2 thin films on p-Si (100) substrate is depicted in Fig. 2. A smooth, homogenous, uniform and crack-free surface with small roughness was observed. The root mean square (RMS) roughness value of the films deposited in this study was found 9 Å which is a quite low value and in expectable range for the CMOS applications [1].

The XPS measurements were performed to explore the chemical composition, valence state of Hf and oxygen vacancy, related defect sites in HfO_2. Figure 3a shows the Hf 4f XPS core level spectra; this can be de-convoluted into three distinct peaks. The binding energies of Hf $4f_{7/2}$ and Hf $4f_{5/2}$ are 16.43 and 18.11 eV, respectively. A small peak at 15 eV is also observed, and this can be assigned to the Hf–Si bond. This concludes the presence of silicate layer at the interface. The separation in Hf 4f peaks indicates the presence of Hf in Hf^{4+} state [22]. Figure 3b shows the O 1*s* XPS core level spectra; this can be de-convoluted into two distinct peaks. The strong XPS signal at 530.2 eV is ascribed to Hf–O bonding of HfO_2. The other peak located at 531.6 eV corresponds to Hf–Si–O bond and verifies the formation of silicate layer as suggested by Hf 4f spectra [23, 24]. The composition of HfO_2 was extracted from the area of the XPS Hf 4f and O 1*s* peaks using CASA XPS software, and it was 1.94.

Figure 4 shows the experimental UPS spectra of HfO_2 films. From the previously published work, we know that the energy difference in elastic peak (e.g., oxygen peak—$E_{O\ 1s}$) and onset of inelastic losses (E_{loss}) corresponds to energy gap (E_g), i.e., $E_g = E_{loss} - E_{O\ 1s}$ [25]. As we can see in Fig. 4, the loss spectra and background zero level intersect at 535.9 eV, i.e., $E_{loss} = 535.9$ eV; as we know from Fig. 4b, the O 1*s* is at 530.2 eV, i.e., $E_{O\ 1s} = 530.2$ eV. Hence, the band gap of HfO_2 films was found 5.7 eV, as shown in the inset of Fig. 4. This is in good agreement with the HfO_2 thin films reported by other techniques and theoretically [6, 27]. The barrier height HfO_2/Si stack is extracted by UPS and XPS (first, electron affinity of HfO_2 is calculated, and this is subtracted from the electron affinity of Si) spectra. We followed the method adopted by Liu et al. [28] and found the electron affinity (χ) 1.88 eV, which is similar to the described in Ref. [29]. From electron affinity, HfO_2/Si barrier height (conduction band offset) is estimated and found to be 2.17 eV. The

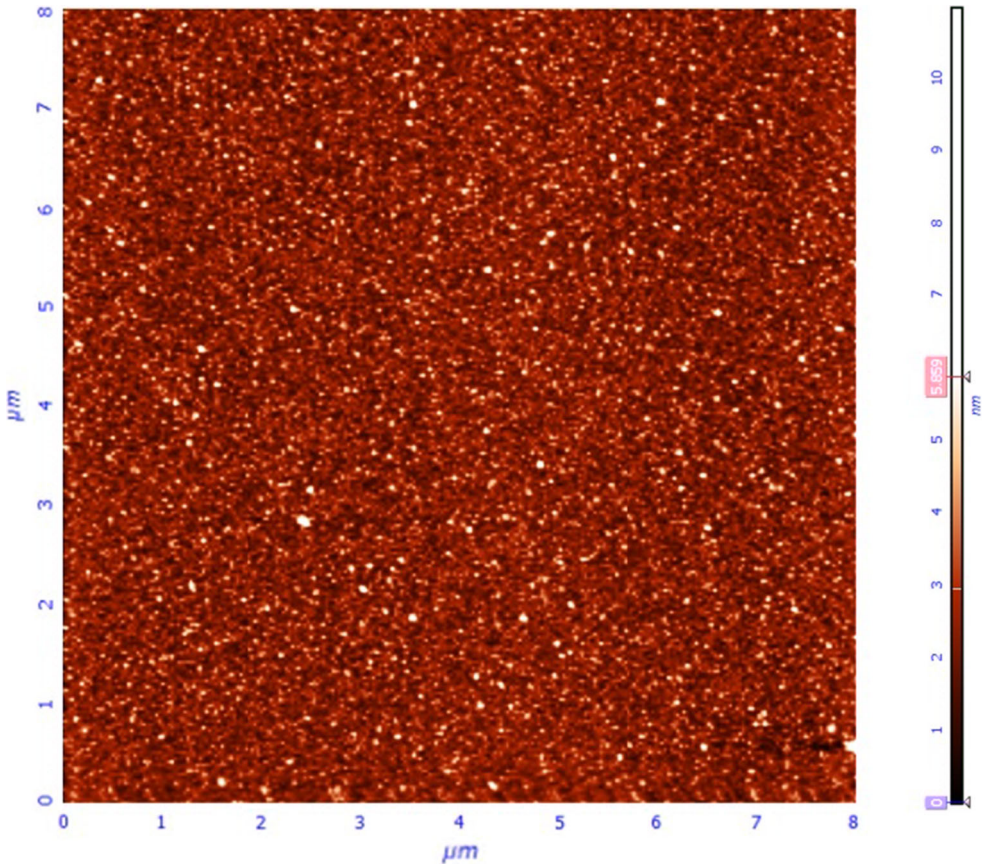

Fig. 2 AFM image of 700 °C-annealed HfO_2 films. The RMS roughness is estimated to be 9 Å

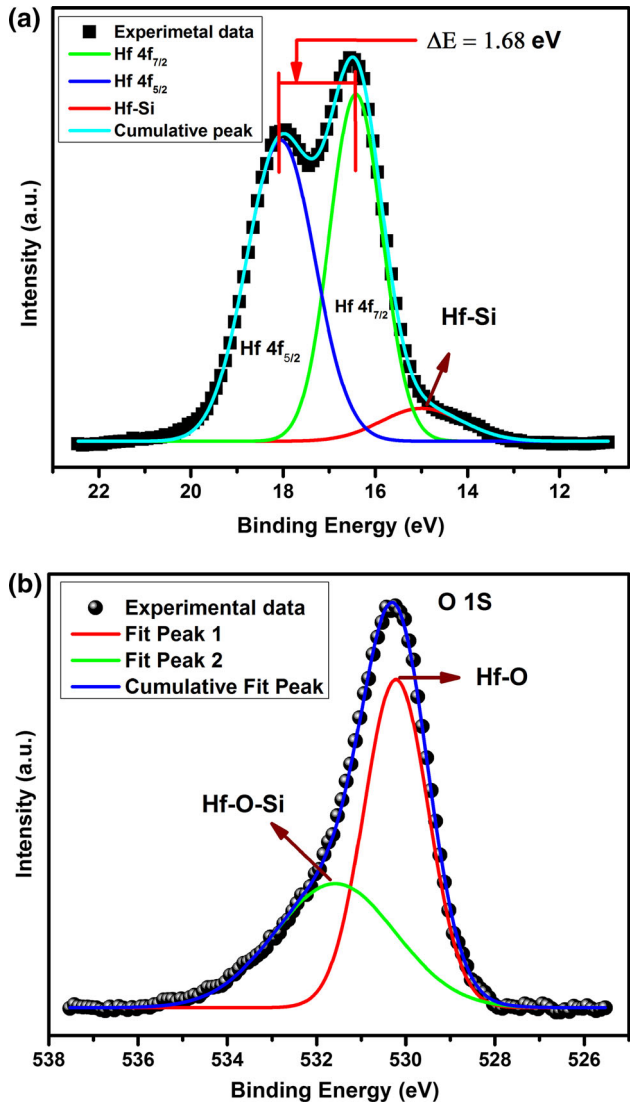

Fig. 3 **a** Hf 4f XPS core level spectra of HfO_2 thin films. The difference of 1.68 in the binding energies of Hf $4f_{7/2}$ and Hf $4f_{5/2}$ suggests Hf in Hf^{4+} state. **b** The O 1*s* spectra of HfO_2 films

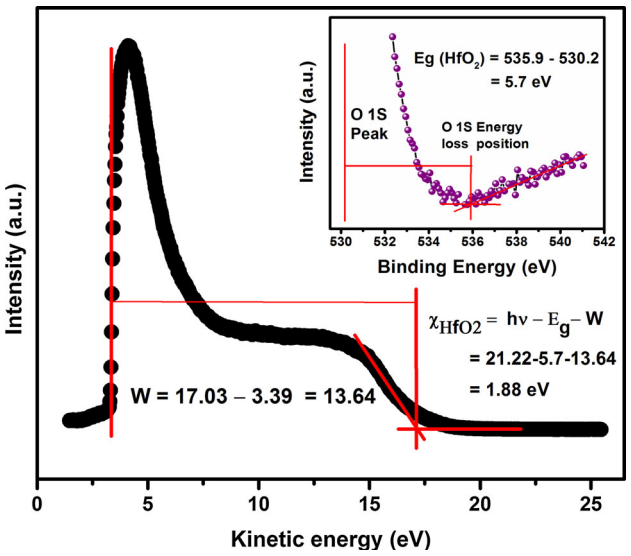

Fig. 4 UPS spectra of HfO_2 thin films. The band gap estimation from the O 1*s* plasmon loss spectra is shown in the inset

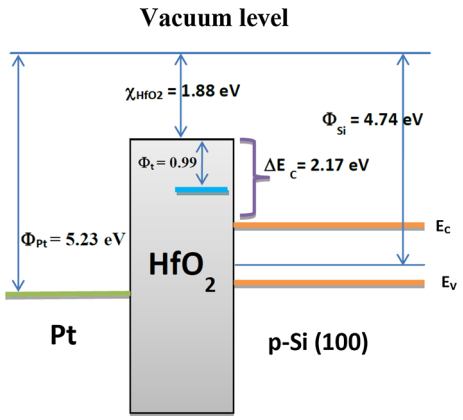

Fig. 5 Simplified band alignment of Pt/HfO_2/p-Si MIS device derived from UPS and XPS spectra. Pt work function on HfO_2 thin films is taken from the Y. C. Yeo article. The trap level at 0.99 eV below the conduction band edge is estimated from the trap-assisted tunneling model

simplified band alignment of Pt/HfO_2/p-Si MIS device is shown in Fig. 5; the Pt work function on the HfO_2 films was taken from Ref. [30].

Figure 6 shows the experimental and fitted Ψ–Δ–λ plot of HfO_2 thin film deposited on Si. Fitting the optical constants of thin films with a Cauchy dispersion model by spectroscopic ellipsometry (SE) parameters allows the estimation of thicknesses of the films. The thickness and refractive index were estimated 17 nm and 2.08 at the wavelength of 550 nm, respectively. The refractive index as a function of wavelength is shown in the inset of Fig. 6. The density (ρ) is estimated from the formula; $\rho = 11.36 \quad n - 14.43$ where 'n' is the refractive index at 550 nm wavelength [31]. The 'n' and 'ρ' values are 2.08 and 8.51 g/cm^3, respectively. The density of the films is close to the bulk value (9.68 g/cm^3). The high value of refractive index (or density) proposing a well-packed and pore-free nature of the films.

Figure 7 shows a *C–V* characteristics of Pt/HfO_2/p-Si MIS capacitor at different frequencies from 1 kHz to 1 MHz. The well-behaved *C–V* shows proper accumulation, depletion and inversion regions. The schematic diagram of the MIS structure is depicted in the left-side inset of Fig. 5. The dielectric constants (κ) is calculated from the *C–V* plot using the relation 1:

$$\kappa = \frac{C_{ox} t_{ox}}{\varepsilon_0 A} \tag{1}$$

where C_{ox} is the accumulation capacitance, t_{ox} is the oxide film thickness and ε_0 is the permittivity of free space, and A is the area of the device.

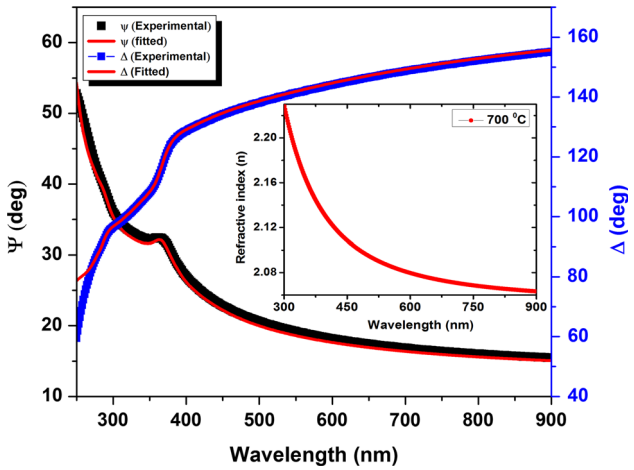

Fig. 6 Experimental and Cauchy dispersion model fitted Ψ–Δ–λ plot of curve of HfO_2 thin film deposited on Si. The refractive index as a function of wavelength extracted from ellipsometery data is shown in the inset. The high value of refractive index at the 550 nm wavelength suggests a well-packed HfO_2 thin film

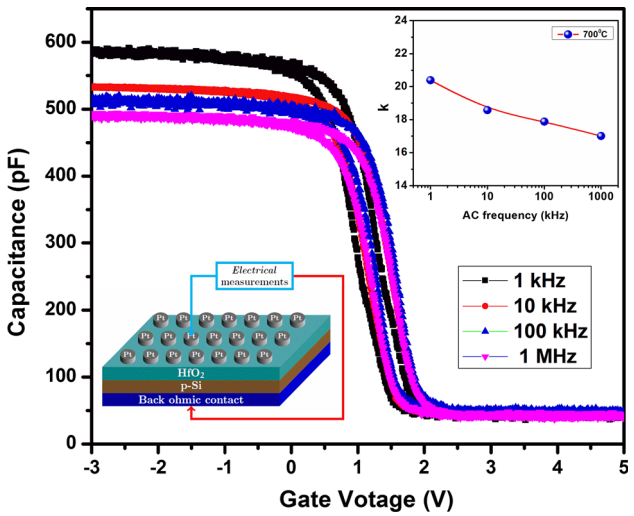

Fig. 7 Capacitance–Voltage (C–V) characteristics of 700 °C-annealed HfO_2 MIS device from 1 kHz to 1 MHz. The schematic diagram and dielectric constant (κ) as a function of frequency are shown in the inset of the figure

The oxide capacitance (C_{ox}), flat band capacitance (C_{FB}), flat band voltage (V_{FB}), oxide-trapped charge (Q_{ot}) calculated from the high-frequency (1 MHz) C–V curve are 490, 241 pF, 1.2 V, 1.8×10^{12} cm^{-2}, respectively. A high dielectric constant 17 at 1 MHz frequency was observed. The dielectric constant as a function of frequencies is shown in the right-side inset of Fig. 7. The dielectric constant changes from 21 to 17 with increasing frequency from 1 kHz to 1 MHz. The dielectric polarization, presence of oxide traps (mainly oxygen vacancies) in the oxide and the presence of interface defect at the interface of Si/HfO_2 are the main reason for the frequency dispersion of dielectric constant [32]. Small frequency dispersion is the indication of good interface and low concentration of traps present in MIS structure.

The leakage current density of 700 °C-N_2-environment-annealed HfO_2 film is shown in Fig. 8a. The asymmetrical nature of current density curve in gate and substrate injection mode is due to the different barrier height faced by the carriers at the Pt/HfO_2 and HfO_2/Si interfaces. A small leakage current density 6.8×10^{-9} A/cm^2 at +1 V was achieved. The improved leakage current density is due to the N_2 environment annealing, growth of the interfacial SiO_x and silicate layer formation in between HfO_2 and Si. The N_2 annealing is reducing the oxygen vacancies concentration and enhancing the stoichiometry. This is also reducing the possibility of oxygen diffusion into the Si due to the quenching of atomic vibration of Si atoms and hence reduces the thickness of interlayer formed during annealing and beneficial to achieve the smaller EOT. For the clear comparison about the quality of our device with previously reported work, various parameters of our device are tabulated in Table 1 and compared with previous work in which devices are fabricated by sputtering and other techniques [8, 9, 16, 39]. In addition to that, as we have prepared a lot of MIS devices, we have selected five to six devices randomly for measurement and we found similar results for each device. We have also repeated the electrical measurement after few months and did not observe any changes in electrical characteristics. Hence, the MIS devices presented in this articles are of high quality, have no variation in performance and show a very good reproducibility.

The leakage current conduction mechanisms of the HfO_2 MIS devices are investigated; numerous conduction mechanisms are dominant at different bias voltages. In gate injection mode, for the low-field region Poole–Frenkel (PF) mechanism dominates and is shown in Fig. 8b. The emission of trapped electrons into the conduction band of HfO_2 is accountable for this and given by

$$J_{PF} = CE \exp\left[-\frac{q\phi_t}{kT} + q\frac{\sqrt{qE/\pi\varepsilon_r}}{kT}\right] \quad (2)$$

where C, E, q, ε_r, k and T are the trap density-related constant, electric field, electronic charge, dynamic dielectric constant, Boltzmann constant and absolute temperature, respectively.

To clarify the PF emission-controlled leakage current in HfO_2 MIS device, a plot of ln (J/V) versus $V^{1/2}$ is depicted in Fig. 8b and it is linear for the small biases voltages. The ε_r value calculated from the slope is 4.91, and this is close to the optical dielectric constant (ε_{op}) obtained from the ellipsometry ($\varepsilon_{op} = n^2 = 4.33$, '$n$' is the refractive of thin film at 550 nm) [33]. Hence, it can be understood that the leakage current in the low-field region is controlled by PF emission.

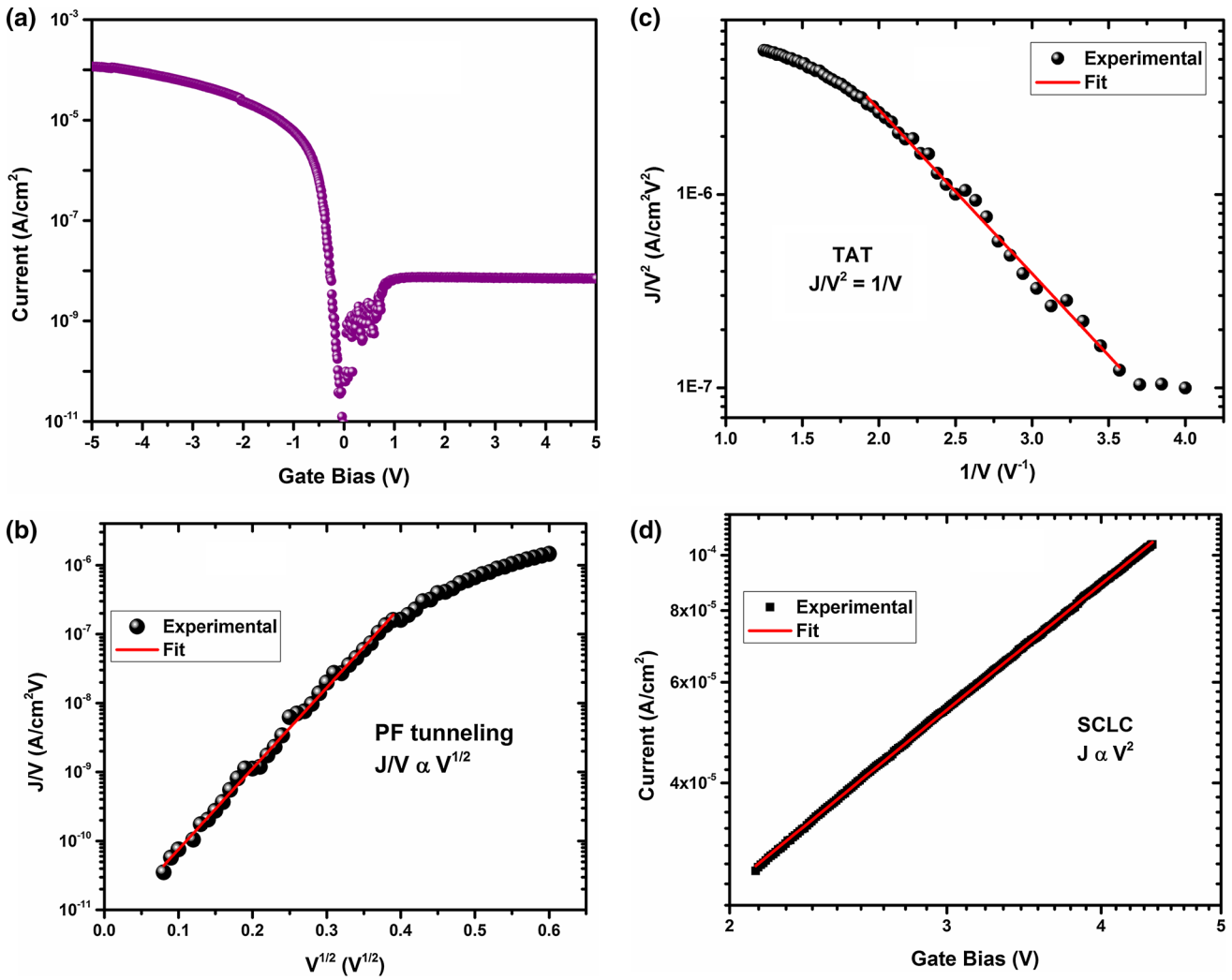

Fig. 8 **a** Semi-logarithmic forward and reverse bias current–voltage curves of the 700 °C-annealed HfO_2 films on p-Si substrate. The asymmetrical nature of current density curve in gate and substrate injection mode is due to the different barrier height faced by the carriers at the Pt/HfO_2 and HfO_2/Si interfaces. **b** PF emission in gate injection mode. **c** The Fowler–Nordheim (FN) tunneling plot of ln (J/V^2) versus $1/V$. **d** The double-logarithmic plot of current density versus the applied voltage at the higher voltages

Table 1 Technology comparison of HfO_2 MIS devices fabricated by various techniques to present work

Fabrication method	Thickness (nm)	Annealing temp. (K)	Dielectric constant (κ)	EOT (nm)	V_{FB} (V)	Leakage current (A/cm^2)	References
E-beam	32	300	19	6.6	−1.6	1.2×10^{-7}	[8]
Sputtering	18	500	15.43	4.5	−0.95	1.6×10^{-5}	[9]
ALD	50	200	15	13	–	1×10^{-9}	[16]
Spin-coating	30	750	10–11	11	−1.1	4×10^{-8}	[39]
Sputtering	17	700	17	3.9	1.21	6.8×10^{-9}	Present work

ALD atomic layer deposition, *E-beam* electron beam deposition, V_{FB} flat band voltage, *EOT* equivalent oxide thickness

Fowler–Nordheim (FN) tunneling-derived leakage current density is expressed as [34],

$$J_{FN} = \frac{q^2}{8\pi h \phi_B} E^2 \exp\left[-\frac{8\pi\sqrt{2qm*}}{3hE}\phi_B^{3/2}\right] \quad (3)$$

where q, h, Φ_B, E and $m*$ are the electronic charge, Plank's constant, barrier height, electric field and effective mass in the oxide layer, respectively.

The FN curve [ln (J/V^2) vs. 1/V] is shown in 8c. Equation 3 is well fitted in intermediate region. The barrier

heights (Φ_{FN}) are estimated to be 0.99 eV. The oxygen vacancy is the main electron defect site in HfO_2. In HfO_2/Si system, oxygen vacancy can transfer electron into the Si and become positively charged, for example to acceptor states, even if there is no interstitials. The trap related to oxygen vacancies lies just above the Si conduction band edge, and positions of trapping levels below the oxide conduction band edge depend on the annealing temperature, deposition and calculation methods [35–38]. The trap activation energy (0.99 eV) is very close to fourfold oxygen vacancies-related defect (1.18 eV) as described by Chen et al. [26]. In their study, the band gap was 5.94 eV and the band gap of our film is 5.7 eV. Moreover, the difference in Φ_t value is 0.19 eV and the difference in band gap is 0.24 eV. Hence, we can assign this trap level to fourfold oxygen-related vacancy traps.

A strong accumulation layer formed in the Si vicinity for the high voltages. Space-charge-limited current (SCLC) controlled the current density at higher voltages and given by [34]

$$J_{SCLC} = \frac{9}{8}\varepsilon_i \mu\theta V^2 d^{-3} \quad (4)$$

where ε_i is the permittivity of oxide, μ is the mobility, θ is the ratio of free to shallow trapped charge, V is the voltage, and d is the thickness of the oxide layer.

Figure 8d depicts the ln (J) versus ln (V) plot. The plot is linear with the exponent 1.79, which is very close to 2. This suggests nearly power law dependence for the higher bias voltage. As suggested previously that SCLC mechanisms can be verified if the $\mu\theta$ multiplication is small due to the low carrier mobility in the oxide layer and large number of trap occupancy [34]. From the experimental current densities (J) versus voltage plot and using Eq. 4, the $\mu\theta$ product was found to be 10^{-10} cm^2 V/s, which is quite low value. We can suggest that SCLC controls the current conduction at the higher voltage region despite ultra-thinness of dielectric layer. Hence, it can be concluded that the SCLC mechanism is governing the leakage current in this region.

4 Conclusions

High-quality HfO_2 thin films successfully integrated in MIS device. MIS capacitor was fabricated, structural, optical, electrical and dielectric properties have been investigated. A smooth surface and high dielectric constant ($\kappa = 17$) at 1 MHz was estimated in the present study. Equivalent oxide thickness (EOT) and leakage current density are found to be 3.9 nm and 6.8×10^{-9} A/cm^2 at +1 V. The improved leakage current density is due to the N_2 environment annealing, growth of the interfacial SiO_x and silicate layer formation in between HfO_2 and Si. The N_2 annealing is reducing the oxygen vacancies concentration and enhancing the stoichiometry. The band gap of the film is estimated from O 1s loss spectra and found to be 5.7 eV. The electron affinity (χ) and HfO_2/Si barrier height (conduction band offset) extracted from UPS spectra are 1.88 and 2.17 eV, respectively. A trap state with 0.99 eV activation energy below the conduction band edge is found and assigned to the fourfold coordinated oxygen vacancy in m-HfO_2.

Acknowledgements AK would like to thank UGC, New Delhi, for the research fellowship.

References

1. G.D. Wilk, R.M. Wallace, J.M. Anthony, J. Appl. Phys. **89**, 5243 (2001)
2. A. Kumar, S. Mondal, K.S.R.K. Rao, AIP Adv. **5**, 117122 (2015)
3. S. Mondal, V. Venkataraman, IEEE Electron Dev. Lett. **37**, 396 (2016)
4. V. Fiorentini, G. Gulleri, Phys. Rev. Lett. **89**, 266101 (2002)
5. P.K. Nayak, J.A. Caraveo-Frescas, Z. Wang, M.N. Hedhili, Q.X. Wang, H.N. Alshareef, Sci Rep **4**, 4672 (2014)
6. M. Esro, G. Vourlias, C. Somerton, W.I. Milne, G. Adamopoulos, Adv. Funct. Mater. **25**, 134 (2015)
7. H. Wang, Y. Wang, J. Zhang, C. Ye, H.B. Wang, J. Feng, B.Y. Wang, Q. Li, Y. Jiang, Appl. Phys. Lett. **93**, 20 (2008)
8. K.L. Ganapathi, N. Bhat, S. Mohan, Appl. Phys. Lett. **103**, 1 (2013)
9. J. Gao, G. He, J.W. Zhang, B. Deng, Y.M. Liu, J. Alloys Compd. **647**, 322 (2015)
10. I. Park, Y. Choi, W.T. Nichols, J. Ahn, Appl. Phys. Lett. **98**, 19 (2011)
11. D. Lembke, A. Kis, ACS Nano **6**, 11 (2012)
12. I. Karaduman, Ö. Barin, D.E. Yıldız, S. Acar, J. Appl. Phys. **118**, 1 (2015)
13. I. Oh, J. Tanskanen, H. Jung, K. Kim, M.J. Lee, Z. Lee, S. Lee, J. Ahn, C.W. Lee, K. Kim, H. Kim, H. Lee, Chem. Mater. **27**, 5868 (2015)
14. K. Zou, X. Hong, D. Keefer, J. Zhu, Phys. Rev. Lett. **105**, 1 (2010)
15. M. Liao, H. Ishiwara, S.I. Ohmi, IEEE Trans. Electron Dev. **61**, 2 (2014)
16. X.-H. Zhang, S.P. Tiwari, S.-J. Kim, B. Kippelen, Appl. Phys. Lett. **95**, 223302 (2009)
17. W.-J. Yoon, P.R. Berger, Org. Electron. **11**, 1719 (2010)
18. R. Zhang, P. Huang, N. Taoka, M. Yokoyama, M. Takenaka, S. Takagi, Appl. Phys. Lett. **052903**, 3 (2016)
19. J.S. Meena, M.-C. Chu, S.-W. Kuo, F.-C. Chang, F.-H. Ko, Phys. Chem. Chem. Phys. **12**, 2582 (2010)
20. Y. Wang, H. Wang, C. Ye, J. Zhang, H. Wang, Y. Jiang, A.C.S. Appl, Mater. Interfaces **3**, 3813 (2011)
21. G.S. Chaubey, Y. Yao, J.P.A. Makongo, P. Sahoo, D. Misra, P.F.P. Poudeu, J.B. Wiley, RSC Adv. **2**, 9207 (2012)
22. J.M. Chem, C. Avis, Y.G. Kim, J. Jang, J. Mater. Chem. **22**, 17415 (2012)
23. L. Qi, B. Cheng, J. Yu, W. Ho, J. Hazard. Mater. **301**, 522 (2015)
24. J. Liu, M. Liao, M. Imura, A. Tanaka, H. Iwai, Y. Koide, Sci. Rep. **4**, 6395 (2014)

25. M.T. Nichols, W. Li, D. Pei, G.A. Antonelli, Q. Lin, S. Banna, Y. Nishi, J.L. Shohet, J. Appl. Phys. **115**, 094105 (2014)
26. T.-J. Chen, C.-L. Kuo, J. Appl. Phys. **110**, 064105 (2011)
27. M.C. Cheynet, S. Pokrant, F.D. Tichelaar, J. Rouvière, J. Appl. Phys. **101**, 1 (2007)
28. Z.Q. Liu, W.K. Chim, S.Y. Chiam, J.S. Pan, C.M. Ng, J. Mater. Chem. **22**, 17887 (2012)
29. H. Borkar, A. Thakre, S.S. Kushvaha, R.P. Aloysius, A. Kumar, RSC Adv. **5**, 35046 (2015)
30. Y.-C. Yeo, T.-J. King, C. Hu, J. Appl. Phys. **92**, 7266 (2002)
31. M. Jerman, Z. Qiao, D. Mergel, Appl. Opt. **44**, 3006 (2005)
32. A. Kumar, S. Mondal, K.S.R.K. Rao, J. Mater. Sci.: Mater. Electron. **27**, 5264 (2016)
33. A. Kumar, S. Mondal, K.S.R.K. Rao, Appl. Surf. Sci. **370**(373), 373 (2016)
34. S.M. Sze, *The Physics of Semiconductor Devices*, 2nd edn. (Wiley, New York, 1981), pp. 402–406
35. M. Jain, J.R. Chelikowsky, S.G. Louie, Phys. Rev. Lett. **107**, 1 (2011)
36. K. Xiong, J. Robertson, M.C. Gibson, S.J. Clark, Appl. Phys. Lett. **87**, 183505 (2005)
37. P. Broqvist, A. Alkauskas, A. Pasquarello, Appl. Phys. Lett. **92**, 132911 (2008)
38. J. Ni, Q. Zhou, Z. Li, Z. Zhang, Appl. Phys. Lett. **93**, 011905 (2008)
39. K. Suzuki, K. Kato, J. Appl. Phys. **105**, 1 (2009)